Role of Planar Laser-Induced Fluorescence in Combustion Research.

F. Grisch, M. Orain

Frédéric Grisch,
Mikaël Orain
(Onera)

E-mail: frederic.grisch@onera.fr

Role of Planar Laser-Induced Fluorescence in Combustion Research

Laser diagnostics are now considered an indispensable tool in fluid dynamics research. Such measurements provide a deeper understanding of the inner physical and chemical processes, which is required to validate and improve computer-based simulations and to assist applied research in practical combustors. This paper presents an overview of the potential of planar laser-induced fluorescence (PLIF), which currently allows for the imaging of scalar properties such as species concentration, temperature, velocity, pressure and density over wide pressure and temperature ranges with high temporal and spatial resolution. Although a complete picture of the present research and PLIF applications to fluid mechanics is beyond the scope of this article, this overview focuses rather on the basic concepts underlying the technique and its application to various flowfields at Onera. These examples cover applications to primarily gas flows like mixing experiments under isothermal and isobaric conditions, fuel/air mixing and temperature measurements in heated jet flows, subsonic and supersonic flame structures and improvement of combustion processes using nanosecond pulsed discharges. Several examples of measurements of fuel concentration in multiphase flows, flame structure around isolated droplets and fuel/air mixing processes in kerosene/air combustion at high pressure are presented. The paper concludes with a section that addresses key issues that remain as challenges for continued research towards the improvement of quantitative PLIF measurements.

Introduction

Knowledge of the physics and modeling of turbulent gaseous and reacting flows is constantly progressing. Detailed information is vital to demonstrate the reliability of the various numerical models already developed and to further improve their prediction capabilities in order to increase combustor performances. Since the advent of the laser in the early 60's, various laser-based spectroscopic techniques have been developed for diagnostic purposes. These methods are extremely valuable for probing harsh environments such as turbulent flames, where non-intrusive optical techniques with high spatial and temporal resolution are very useful. Among the various laser-based diagnostics currently employed, imaging techniques including planar laser-induced fluorescence (PLIF), Raman, Rayleigh, and Mie scattering have proven useful in a wide variety of flows [1-3]. The resolved image can reveal important information about the structure of the flow and/or the combustion processes that influence combustor design. Spatially-resolved measurements are obtained over a large number of points included in the laser sheet, thereby providing an instantaneous image of the flowfield properties. A detailed study of large- and small-scale structures within the image is possible in both reacting and non-reacting flows, as well as fundamental studies dealing with the validation of turbulent flow modeling.

PLIF imaging is one of the most promising of these techniques because it is species- and quantum state-specific, and is therefore sensitive to species composition, temperature, number density and velocity. The other advantage of PLIF is its ability to provide instantaneous information over the whole plane of the flowfield, without the light-of-sight averaging inherent to the Schlieren and Shadowgraph techniques. Signals are higher than those of Rayleigh and Raman scattering, while the use of atomic or molecular fluorescent species generally ensures that the tracer is a suitable marker of the flow. Since its initial development in the late 70's and early 80's [4, 5], the potential of PLIF has been demonstrated in a wide variety of environments [6-8]. Achieving quantitative PLIF measurements can be very challenging, primarily because the effects of collisional quenching must be considered in the signal analysis. However, several strategies have been developed to either account for or to minimize the effects of collisional quenching. For instance, quantitative time-averaged imaging

of concentration, temperature, pressure and velocity has been demonstrated in compressible flows [2]. Temporally-resolved imaging of concentration and temperature has also been demonstrated in a non-reacting jet and flame, respectively, but detailed instantaneous two-dimensional property measurements in complex mixing and turbulent combustion flows were limited. While time-averaged measurements are useful for validation of computational models, there is a clear need for instantaneous imaging measurements in realistic mixing and combustion flowfields. For instance, temporally-resolved measurements are needed for a better understanding of the flow physics, leading to improved modeling of turbulent mixing mechanisms and the interaction between turbulence and combustion [55] Instantaneous measurements are also particularly relevant in light of the importance of large-scale structures in turbulent mixing and combustion [9]. Therefore, the need to better understand the instantaneous structure of a given flow, which ultimately governs combustion processes, provides a strong motivation for the continued development and application of temporally-resolved PLIF techniques.

This paper first provides a brief general background for the PLIF technique and references to relevant literature. Practical considerations and a selection of fluorescent tracers are then discussed in the second part of the article. In the third part, examples covering PLIF applications in mono- and two-phase reactive flowfields are presented. Finally, the paper concludes with a section that addresses key issues that remain as challenges for continued research towards the improvement of quantitative PLIF measurements.

Fundamentals

Theory

Fluorescence denotes the radiation emitted by an atom or a molecule when it relaxes by spontaneous emission of a photon from a higher to a lower energy level. In laser-induced fluorescence (LIF) processes, the upper energy level is populated using laser excitation with a wavelength tuned to a resonance between the excited state and a discrete lower state. Typically, the lower state is in the ground electronic level, as the other electronic states may be negligibly populated at combustion temperatures. For more detailed information about LIF, see [3,7,8].

After excitation, the laser-populated upper state may undergo a number of subsequent processes. First, the molecule can return to the ground state by laser-induced, stimulated emission. Second, absorption of an additional photon can excite higher molecular states, including ionized levels. Third, the internal energy of the system can be altered via inelastic collisions with other molecules, producing rotational and vibrational energy transfer, together with electronic energy transfer; the latter is often referred to as quenching. Fourth, interactions between the separate atoms of the molecule, known as “internal” or “half” collisions, produce internal energy transfer and dissociation of the molecule. When the dissociation is produced by a change between a stable and a repulsive electronic arrangement in the molecule, it is called predissociation. Finally, the originally populated state, and nearby upper states, are indirectly populated through collisions and fluoresce, producing the LIF signal.

LIF signals can be related to specific properties (concentration and temperature) of the absorbing species through modeling of these state-to-state transfer processes. As fluorescence is a function of the upper state’s population, such modeling requires solving the state-dependent population dynamics. While quantum-mechanical density-matrix descriptions of the interactions involved in LIF are available [10-11], most treatments of LIF are based on a semi-classical rate equation analysis [12]. Generally, a simplified treatment of this rate equation is used. It consists of a two-level molecular system, where the two levels are those probed by the laser radiation.

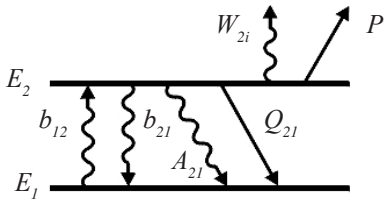

Figure 1 - Energy level diagram for a two-level fluorescence model

Figure 1 displays the rate constants for the different optical and collisional processes connecting the upper and lower energy levels, E_1 and E_2. b_{12} corresponds to absorption and b_{21} to stimulated emission, b_{12} and b_{21} are related to the Einstein coefficients for stimulated emission and absorption, B, through $b = BI_\nu / c$, where I_ν is the incident laser spectral irradiance. A_{21} (given by the Einstein A coefficient) is the rate constant for spontaneous emission, which represents the fluorescence signal. P corresponds to predissociation and W_{2i} to photo-ionization. These processes are generally negligible and they are not considered here. Q_{21} corresponds to the collisional quenching. This term represents the de-excitation that the molecule undergoes based on inelastic collisions with other molecules. It is described by:

$$Q_{21} = N\sum_i \chi_i \sigma_i v_i \tag{1}$$

In this expression, N represents the total number density, χ_i the collider species mole fraction, σ_i the collision cross section (species dependent) and v_i the mean molecular speed between the absorbing species and colliding species.

The rate equations for the population densities of the two energy levels, N_1 and N_2 are then expressed by:

$$\frac{dN_1}{dt} = -N_1 b_{12} + N_2(b_{21} + A_{21} + Q_{21}) \tag{2}$$

$$\frac{dN_2}{dt} = N_1 b_{12} - N_2(b_{21} + A_{21} + Q_{21}) \tag{3}$$

As commonly suggested, the upper level has a negligible population prior to the laser excitation, so the initial condition, $N_2(t=0)=0$. Additionally,

$$N_1 + N_2 = N = N_1^0 \tag{4}$$

where N_1^0 represents the initial population of N_1. Resolution of Eqs. 2 and 3 yields the following expression for N_2:

$$N_2(t) = \frac{b_{12} N_1^0}{(b_{12} + b_{21} + A_{21} + Q_{21})}(1 - e^{-\tau t}) \tag{5}$$

Where the time constant τ is equal to $1/(b_{12} + b_{21} + A_{21} + Q_{21})$. For laser pulses that are long compared to τ (10 ns vs. ~ 1 ns), the system reaches steady state with N_2 equal to:

$$N_2 = N_1^0 \frac{b_{12}}{(b_{12}+b_{21})} \frac{1}{1+\dfrac{A_{21}+Q_{21}}{b_{12}+b_{21}}} = N_1^0 \frac{B_{12}}{B_{12}+B_{21}} \frac{1}{1+\dfrac{I_\nu^{sat}}{I_\nu}} \quad (6)$$

where I_ν^{sat}, is the saturation irradiance defined as:

$$I_\nu^{sat} = \frac{(A_{12}+Q_{12})}{B_{12}+B_{21}} \quad (7)$$

The fluorescence rate is finally converted to a total fluorescence signal by temporal integration over the laser pulse duration and by taking into account the collection efficiency of the detection optics. Assuming the fluorescence is emitted equally over 4π steradians, the total number of photons N_p detected by a photo-detector from the collection volume V is:

$$N_p = \eta \frac{\Omega}{4\pi} f_1(T) \chi_m n V B_{12} E_\nu \frac{A_{21}}{A_{21}+Q_{21}} \quad (8)$$

η is the transmission efficiency of the collection optics, Ω is the solid angle of collection, $f_1(T)$ is the fractional population of the lower-coupled state, χ_m is the mole fraction of the absorbing state, n is the total gas number density and E_ν is the spectral fluence of the laser. The term $A_{21}/(A_{21}+Q_{21})$ is called the Stern-Volmer factor or fluorescence yield. It is generally much smaller than 1 as $A_{21} << Q_{21}$. In order to perform quantitative measurements of species concentrations in the linear regime, the quenching rate constant must be evaluated. The quenching rates can be calculated in various flames using available data for the specific quenching cross sections and weighting by the mole fractions of species in the gas mixture. For some cases, the fluorescence signal can be independent of quenching, which allows for quantitative LIF measurements. If the laser irradiance is increased until $I_\nu >> I_\nu^{sat}$, the fluorescence signal also becomes independent of both laser irradiance and quenching. However, these conditions are difficult to obtain in the spatial, temporal, and spectral wings of the laser pulse, which precludes the use of this approach in most situations.

Planar imaging: practical considerations

Several requirements must be satisfied in order to perform quantitative measurements on a given species. First, the molecule needs to have a known absorption and emission spectrum. Second, the rate of radiative decay of the excited state, which directly influences the fluorescence signal, must be known. Third, all the excited state losses, mainly coming from collisions, photo-ionization and predissociation, must be taken into account. Several measurement strategies including one and two-wavelength excitation techniques have been specifically developed to measure species concentration and temperature. When mole fraction has to be measured, a single-wavelength excitation scheme can be used [6]. A quantum state is selected to minimize the overall temperature dependence of the fluorescence signal in the temperature range of the experiment, leading then to a direct proportionality between the number density and the fluorescence intensity. Using suitable calibration techniques, the proportionality factor can be evaluated. It depends on the experimental parameters such as observation volume, solid angle, the spectral and spatial efficiencies of filters and cameras, the power density of the laser, spectroscopic constants such as transition probability, absorption lineshape and fluorescence quantum yield, which are usually known. However, the knowledge of the fluorescence quantum yield may be problematic. Pressure, temperature and species composition at the observation volume govern the local collisional-quenching rate and are thus determinant for the fluorescence quantum yield. In flames, when steep gradients of temperature and mixture composition take place, the fluorescence quantum yield can change drastically with position, making quantitative LIF measurements difficult to perform.

Temperature measurements require consideration of several factors including (i) the reduction of the fluorescence signal to a function of temperature only; (ii) a large variation of fluorescence yield with temperature; (iii) the capability of accurate prediction of the fluorescence signal; (iv) high signal levels compatible with the dynamic range of the detection system. A two-line excitation scheme is then selected based on preliminary studies such as [13-14]. In our case, the fluorescence ratio obtained by the sequential excitation of two different initial states of the absorbing molecule was used. The ratio of the fluorescence intensities is then proportional to the relative populations of the corresponding absorbing states and hence is a function of temperature through Boltzmann statistics, assuming a thermodynamic equilibrium. The change of the number density, mole fraction and collisional quenching with temperature can be minimized if the same upper state is selected for both excitations. The technique can be therefore used in a wide range of flowfields, including those that are compressible and/or varying in composition.

The typical arrangement for PLIF measurements is schematized in Figure 2. In the single-line approach, the UV laser beam is tuned to excite a molecular transition. A system of cylindrical and spherical lenses is used to focus the laser beam into a thin sheet. Fluorescence from part of the laser sheet interacting with the flow is collected by an imaging lens at a right angle, and imaged on a gated, intensified CCD camera. A spectral band-pass filter is placed in front of the imaging lens to reject the scattered light and to select the suitable fluorescence. The spatial resolution achievable depends on the pixel size of the detector array, the depth-of-field of the collection optics, the image magnification factor, and the size of the beam waist at the probe volume. A diode array may be used to measure the distribution of laser irradiance over the height of the laser sheet in order to correct the spatial non-uniform laser excitation (flat fielding procedure) as well as to account for drift and fluctuation of the laser energy. A trigger system is required to drive the pulsed laser and the synchronous amplification of the CCD camera over a suitable gate duration. This temporal discrimination improves the rejection of flame luminosity that is partly made by spectral filtering. For the two-line temperature measurements, two lasers are used to excite two different transitions offering the best sensitivity to temperature. The two laser pulses are fired sequentially, with a delay as low as 100 ns to temporally separate the fluorescence decays of each transition. The two Intensified Charge-Coupled Device (ICCD) cameras are gated to integrate the fluorescence signal accordingly.

While two-dimensional images yield a wealth of structural information and give good insight into the physical processes governing the fluid dynamics, in many cases more information is desirable. Multi-species measurements are then of major interest to fully describe the thermodynamic parameters of the observed volume element and to understand correlations between different species concentration and potentially their local variations. The PLIF technique offers the advantage to easily combine with other two-dimensional imaging techniques based on incoherent scattering processes (Raman, Rayleigh,

Mie, LII, etc.). For instance, a Sequential PLIF imaging setup can be used with 2D or 3D (stereoscopic) PIV, with Rayleigh scattering and also with another PLIF system [2]. For these measurements, separate laser sheets were produced from different lasers and these were overlapped in the observed region. Separate detectors were then used to collect the respective signals.

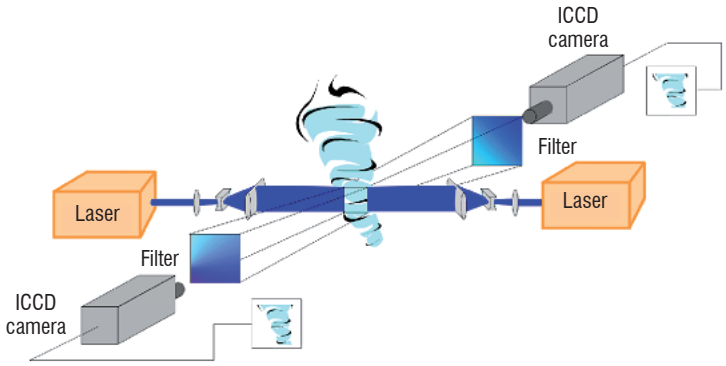

Figure 2 - Schematic representation of a typical experimental set-up for PLIF imaging

Molecular tracers for fluid systems

PLIF diagnostics require the use of fluorescent molecules with well-understood physical and spectral behavior that allows for remote measurements of scalar quantities of interest. Typically, these molecules need to be selected with regard to the physical processes investigated in the flowfield. The following section does not intend to review all fluorescent species detectable in reactive flowfields, but focuses on the main molecules used for the experiments carried out at Onera to yield temporal and spatial information on scalars. In particular, two classes of fluorescent tracers are selected to gain deeper insights into the immensely complex processes prevailing in aeronautic engines such as flow generation, fuel injection and spray formation, mixing, ignition and combustion.

Flame front tracers

The flame front, or reaction zone, is the thin region in a flame where most of the chemical reactions which convert fuel and oxidizer to combustion products take place. These reactions also deliver high local heat release rates which can be also indicators of the flame front. In a non-premixed flame, the flame front separates fuel and oxidizer and in a premixed flame it separates burned and unburned gases. Information about the flame front is essential because it is in the flame region that most of the energy is released, and the total flame front area determines the total amount of energy released in the flame. Assumptions about the properties and structures of flame fronts are part of all turbulent combustion models, e.g. the flamelet approach in RANS modeling or the G-equation approach in LES. The OH radical is the most commonly used flame front indicator. However, other flame front markers such as CH, HCO and the product CH_2O x OH are suitable.

The OH radical is one of the most important intermediate species present in combustors involving air as the oxidizer. OH is formed by fast two-body reactions, such as the attack of H radicals on O_2 molecules, and appears as an intermediate species in many reaction pathways of both hydrogen and hydrocarbon combustion. The OH radical is then consumed by slower three-body recombination reactions [15]. The OH lifetime is particularly long compared to typical fluid-mechanical timescales and, therefore, OH can be convected away from its production location by the local flowfield. OH concentrations are large in the lean regions of the flame front, where chemical reactions involved in the combustion process are completed. In a premixed flame, OH produced in the flame front is slowly consumed in burnt gases, and thus remains present in the burnt gas region at equilibrium concentrations. In a non-premixed flame, OH marks a wider region of the flame front than for instance the CH radical. From studies of flame-vortex interactions, it is also found that the peak of OH concentrations can nevertheless be used as a reliable indicator of heat release and flame front position. However, care has to be taken in situations of large unsteady flame curvature, conditions for which this is no longer valid [16].

CH is produced during the initial reaction of hydrocarbons and air and then rapidly decays as the products of these fast reactions are converted into other species. The CH profile is therefore relatively thin and represents the fuel rich side of the flame where fuel consumption is initiated [15]. Chemical kinetic computations and experiments have also shown that the HCO radical concentration closely matches the distribution of heat release, making it an ideal tracer of the flame front [16]. HCO is an important radical for the oxidation of hydrocarbons in combustion processes. It is formed by CH_2O, and reacts with almost every other molecule in the flame to yield CO and other radicals. The place of HCO in combustion mechanisms makes it a direct link to the overall rate of fuel consumption, and it is also a fast dissociating species which makes its concentration approximately equal to its production rate. These two factors correlate well with the heat release. However, single-shot HCO-PLIF measurements are difficult due to the low concentration of this molecule and its fast predissociation. The product of OH and CH_2O can also be a good alternative because it correlates well with the local heat release rate, and the measured heat release allows for determination of the position of the flame front. It can be shown that the product of OH and CH_2O concentrations is proportional to the reaction rate of the reaction $CH_2O+OH \rightarrow H_2O+HCO$, over a limited temperature range. The rate of this reaction reveals a strong correlation with the global heat release rate as for the HCO concentration [17].

Fuel tracers

Fuel concentration distribution is one of the most important parameters to measure in industrial combustors, e.g. gas turbines or IC engines. In general, most gaseous fuels do not fluoresce as opposed to commercial liquid fuels (kerosene, gasoline, etc.), which fluoresce when excited by UV radiation. However, as commercial liquid fuel is a mixture of a large number of hydrocarbons, the fluorescence dependence on pressure and temperature, and the quenching behavior are generally unknown. Furthermore, the absorption and fluorescence properties vary with the composition from batch to batch. For these reasons, the preferred fuel visualization approach consists of using a single-component reference fuel for optical studies in combustors. The use of a pure fuel is also advantageous for comparisons between experiments and numerical simulations which become intractable for complex fuel mixtures. Fuel visualization is then performed using fluorescence from tracer molecules added to a non-fluorescing fuel. These tracers should meet several criteria. The tracer has to be soluble with the liquid fuel and it must behave like the fuel from the liquid phase to the gas phase, so the evaporation characteristics must be similar. In addition, the diffusion behavior of the fuel and tracer molecules must be equivalent. In most imaging experiments, it is not possible to resolve the regions of diffusive mixing. However, the effect of differential diffusion on the composition of the combustion products

can be important in flows where mixing timescales are longer than chemical timescales (high Damköhler number). In a combustion environment, the reaction characteristics such as the pyrolysis rate or auto-ignition temperature of the tracer must not differ much from the fuel. Finally, the tracer must not have a significant influence on the combustion process.

The fluorescent tracers commonly used in these experiments are aliphatic molecules [18]. Species containing chromophores that allow excitation into stable energy states that subsequently fluorescence are selected. This class of molecules includes ketones (R_2CO), aldehydes (R-CHO) and amines (R_3N), where R is a saturated aliphatic hydrocarbon chain. Ketones are most frequently used. Their spectroscopic properties have been thoroughly investigated and they have been applied to various practical systems. Due to their high vapor pressure, acetone (CH_3COCH_3) or 3-pentanone (diethyl-ketone, $[CH_3CH_2]_2CO$) are ideal tracers for gaseous flows. These tracers have transitions which can be easily excited with commercial lasers and the fluorescence, which is shifted to the red, is spectrally well-separated from the absorption spectrum. These species absorb in the near ultraviolet spectral region, with a maximum absorbance around 280 nm. Their fluorescence spectrum is broadband, extending from 330 nm to 600 nm, with a peak around 430 nm. 3-pentanone has been widely used to trace iso-octane in spark-ignition (SI) engines [19], as the evaporation characteristics of the two compounds match very well. Acetone has also been used to trace iso-octane in SI engines [20] or in practical combustors as a tracer of unburned fuel. Nonetheless, at temperatures above 1000 K, acetone starts pyrolyzing and reacts with radicals such as H, O and OH [21-22]. Therefore, differences of chemical behavior between acetone and the fuel must then be considered. Indeed, the pyrolysis rate of acetone is found to be higher than that of hydrogen and methane, but comparable with that of heavier hydrocarbons, e.g. ethane and propane. This limitation prevents the use of acetone in high-temperature, long residence time hydrogen or methane flows, but presents no drawbacks with heavier hydrocarbon fuels. When combustion takes place, the overall rate of destruction of acetone, hydrogen and hydrocarbons by radical attacks are similar. Differential diffusion also represents a limitation when light fuels such as hydrogen or methane are used, but for heavier hydrocarbon fuels, with molar weights closer to acetone, the effects are not significant.
Aromatics are the second family of attractive fluorescent tracers because of their natural presence in commercial fuels. These species exhibit interesting features such as a strong absorption in the UV and thus large fluorescence emission. For instance, single-ring aromatics like 1,2,4-trimethylbenzene and two-ring aromatics like naphthalene and its derivatives can be used to trace kerosene vapor. They typically have high fluorescence quantum yields and their absorption and emission spectra shift towards the red with increasing size of the aromatic structure. The wide variety of molecular sizes and, therefore, boiling points, makes this class of molecules attractive as tracers that can be adjusted to the evaporation behavior of the fuel or that are representative for vaporization classes in multi-component fuels. Another feature of these aromatics is the strong quenching of fluorescence with oxygen. The fluorescence signal intensities do not only depend on the tracer concentration but also on the oxygen molar fraction. As a result, fluorescence from aromatics is found to be proportional to the fuel/air ratio, which is a parameter of major interest to industrials [23].

Gas-phase applications

Mixture fraction / temperature imaging

Improving the extent of the mixing between fuel and air is of great importance in order to increase the combustion efficiency of aircraft engines:
• in terms of pollutant emissions (NOx, COx, soot), which can be greatly reduced if the spatial distribution of the air/fuel mixture in the combustor is homogeneous with a lean equivalence ratio,
• in terms of combustion instabilities, which are known to partly depend on temporal and spatial inhomogeneities of the air/fuel mixture in the combustion chamber.
Quantifying the mixing between fuel and air can be realized by measuring the local mixture fraction or the equivalence ratio in a flow using quantitative PLIF measurements [24]. These parameters characterize the spatial distribution of fuel and air all over the flowfield. Although realistic combustors do not operate at isothermal conditions, studies of mixing processes under such conditions are valuable to assess the validity of computational fluid dynamics (CFD) simulations in specific geometries, thus adding credibility to predictions under non-isothermal conditions.

Figure 3 represents typical instantaneous images of local mixture fractions measured by acetone-PLIF, recorded in an isothermal micro-channel for various Reynolds numbers. This micro-channel is used as a premixing duct and it is placed upstream from a micro-combustion chamber where the fuel/air mixture from the micro-channel is injected and burnt. The aim of the experiment is to better understand mixing and combustion in small volumes ($\sim$ 2 cm^3). The micro-channel is 1.2 mm high and 30 mm long. The airflow comes from the left hand side and a propane airflow seeded with acetone vapor is injected from the top through a 0.5 mm diameter hole. The air flow rate is between 0.3 and 1.5 g/s. In the present case, acetone is used as a fuel tracer to characterize the mixing of fuel with air. High-magnification optics is used in this experiment and the challenge here is to be able to visualize flow structures at the smallest turbulence length scales. With this set-up, the image size is 8x1.2 mm^2 and the spatial resolution of the technique is 14 μm. It is measured on a target of known size where lines with known thickness are drawn, which allows us to estimate the spread function due to the intensifier.

As the Reynolds number (Re) increases, the flow exhibits a transition from laminar to turbulent cases. For Re=100, the flow is laminar and the fuel spatial distribution shows little fluctuation with time and the morphology of the fuel jet remains constant. As can be seen, the fuel/air mixing is very poor and this indicates that combustion using a fuel/air mixture from this micro-channel would have low efficiency. The laminar/turbulent transition is observed for Re=250, where coherent structures start appearing, which influences the fuel jet and the subsequent fuel spatial distribution. For Re=500, strong vortices are observed, which leads to reduction of the mixing length in the micro-channel, hence to improved fuel/air mixing. Such a configuration leads to more homogeneous fuel/air mixing and subsequent combustion would exhibit high efficiency. Images such as those in figure 3 are used to validate micro-mixing models implemented in Onera's proprietary CFD code.

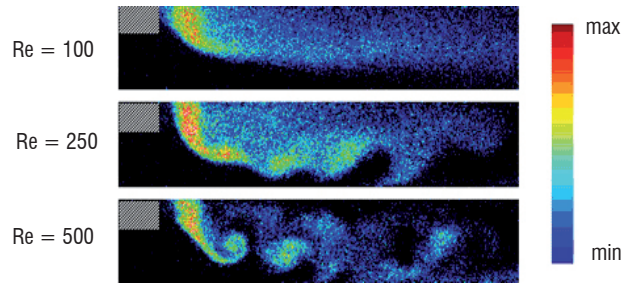

Figure 3 - Single-shot acetone-PLIF images of mixture fraction in a micro-mixing channel for various Reynolds numbers. The air flowrate is between 0.3 and 1.5 g/s, and the size of the image is 8x1.2 mm^2 [24]

A second application of acetone-PLIF is dedicated to temperature measurements in gaseous flowfields. The investigation of a heated turbulent jet is chosen to provide a good test case, which requires the optical diagnostic to have the ability to capture instantaneous temperature and concentration structure on small turbulence length scales. The specific flow considered is a 40 ms^{-1} turbulent jet of acetone-seeded air emanating from the 10 mm diameter nozzle of an electrical air heater with outlet temperature up to 1000 K. The jet is seeded with 3 % acetone, by bubbling part of the cold air stream through liquid acetone and adding it to the heated air immediately downstream from the electrical heater, preventing any acetone pyrolysis. The 266/308 nm dual excitation scheme was chosen because of its good temperature sensitivity within the range of temperature under investigation [22, 25]. Laser sheets at 266 nm and 308 nm, from a quadrupled frequency Nd:YAG and a XeCl excimer laser respectively, are located on the jet centerline just above the nozzle; the excimer laser pulse is delayed by 500 ns relative to the Nd:YAG pulse. Each laser sheet is focused down to a 0.3 mm thickness with a 50 mm height. In order to allow independent control of each sheet, separate focusing sets of lenses are employed in the optical layout. Acetone fluorescence excited by each laser sheet is collected on two separate intensified CCD cameras with a 100 ns temporal gate and the size of the image is 50x50 mm^2. Figure 4 shows typical instantaneous images of acetone molar fraction and temperature results for the heated jet obtained with acetone-PLIF. The turbulence structure of the flow is well captured. In particular, the instantaneous flow structures in the concentration field and temperature images are well correlated with each other.

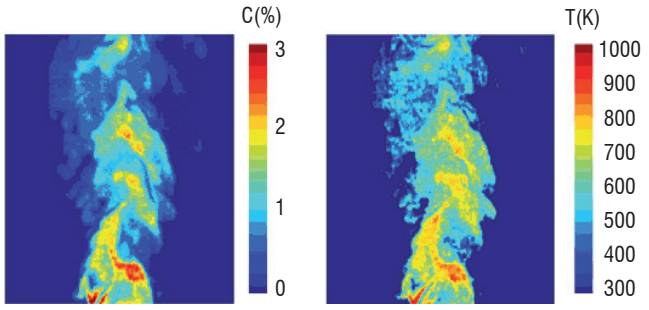

Figure 4 - Instantaneous acetone-PLIF images of acetone molar fraction and temperature in heated turbulent air jet seeded with acetone vapor. The size of the image is 50x50 mm^2

Thermocouple measurements are compared to mean temperatures obtained with 300 frame-averaged acetone-PLIF images and the results are plotted in Figure 5. The radial temperature profiles displayed for different locations downstream from the nozzle show good agreement. Though this flow is not reactive, these results allow for application of acetone-PLIF to reactive flows. In particular, the temperature/mole fraction PLIF described here would be ideal for imaging instantaneous structures in reacting mixing layers, where temperature significantly varies and acetone molar fraction changes because of pyrolysis and radical attack. It could also be useful to image spray flowfields in mixing and/or preheating regions [26].

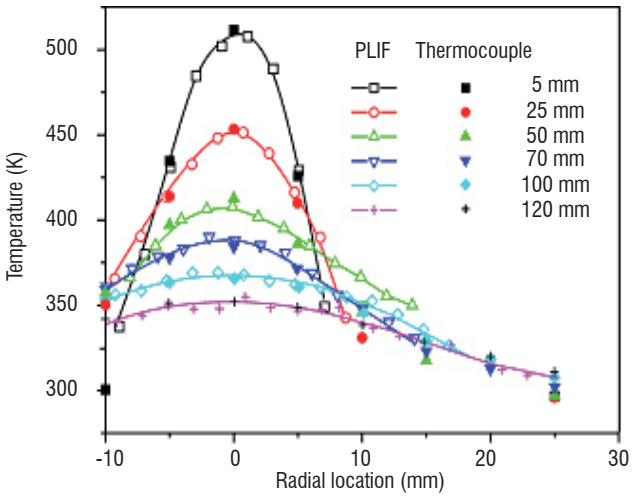

Figure 5 - Radial temperature profiles measured at six axial locations above the nozzle exit: comparison between frame-averaged acetone-PLIF temperature images (open symbols), and thermocouple data (solid symbols)

Subsonic and supersonic combustion

Species concentration measurements are required to study chemically-reacting systems such as flames. Radical number densities can be used to locate reaction zones, or to determine reaction rates. As mentioned before, the hydroxyl radical OH has received considerable attention in the past. For example, the instantaneous spatial distribution of OH is particularly attractive for analyzing the primary reaction zone of a flame. OH-PLIF images can be used to localize regions with high strain where the OH layer becomes thinner and the fluorescence signal is reduced. A useful application of OH-PLIF concerns the investigation of ethylene/air diffusion flames in the pressure range 0.1–0.5 MPa to study the formation of pollutants such as soot and NOx. The flame facility consists of a coflow ethylene/air jet with a concentric premixed ethylene/air pilot flame burner. An example of OH-PLIF images at 0.2 MPa is shown in Figure 6. The whole flame image (300 mm long) is reconstructed from six uncorrelated images (50x50 mm^2) recorded at different axial distances downstream from the injection location. Individual images are obtained using a single pulse with 4 mJ energy and 6 ns duration. The Nd:YAG-pumped dye laser is tuned to excite the Q1(5) line of OH radical at $\lambda = 282.75$ nm in the (1, 0) vibrational band of the $A^2\Pi^+ \leftarrow X^2\Sigma$ system to minimize the temperature dependence. The laser sheet is oriented vertically on the centerline and the size of the region imaged is 50x50x0.2 mm^3. The measurements are performed with jet velocities of 20 and 40 ms^{-1}, corresponding to a Reynolds number between 13000 and 26000. The results shown in Figure 6 provide information on the instantaneous distribution of OH in the central plane of the flame. In particular, it can be shown that the heat release due to the pilot flame stabilizes the shear layer, and the wake region acts as a flame holder providing a source of heat and radicals. Once stabilized, the reaction zone is a continuous filamentary structure where the filaments are often

connected by broader zones. Further downstream from the injector, the presence of broader diffusing OH zones is noticed. Although the OH molar fraction is not precisely known in the present case, the PLIF images can be calibrated by using a well-known reference flame where all parameters are calculated.

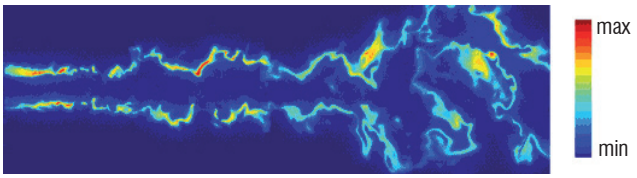

Figure 6 - PLIF images of the instantaneous OH distribution in an ethylene/air flame operating at 0.2 Mpa. The size of the image is 300x50 mm^2

An example of quantitative OH-PLIF is performed in a supersonic flame and results are displayed in Figure 7. The prime purpose is the experimental investigation of combustion in a turbulent reacting mixing layer where finite-rate chemistry effects take place. In the present case, the reactive mixing layer consists of a hydrogen flow at Mach 2 and ambient temperature injected through a cylindrical nozzle (diameter D = 6 mm), and a concentric preheated supersonic air stream at Mach 2 [26]. The probed section is constant over a length of 370 mm and then slightly diverges over 500 mm. The test facility is operated in a blow-down mode because most of its parts are used as a heat sink. Only the main nozzle and the hydrogen injector are water-cooled. The supersonic combustion runs are stabilized for 15 s. The experiments are performed at equivalence ratio (Φ), i.e. the ratio of the fuel-to-oxidizer ratio to the stochiometric fuel-to-oxidizer ratio, of about 0.29. The nominal stagnation air temperature (1800 K) is obtained by an auxiliary hydrogen burner, with oxygen replenishment in order to keep an oxygen molar fraction of 21 % at the inlet of the burner. In order to quantify the fluorescence signals, the raw images are corrected for the dark background and flat field non-uniform response of the camera and the energy and spatial distribution of the laser beam. LIF signals are temperature-dependent and, therefore, the absolute number density of OH needs to be calibrated in a laminar premixed hydrogen/air flame with an equivalence ratio of 0.9, where OH concentration, temperature and pressure are well-known. The reference profile is obtained by recording the fluorescence intensity as a function of the height above the porous burner. Measurements are performed under similar experimental conditions (optical beam path, pulse energy, distance laser/probe volume, ICCD gain, etc.) as for the supersonic combustion experiment. The absolute concentration is retrieved by rescaling the experimental and one-dimensional theoretical profile calculated using the CHEMKIN and PREMIX codes [27, 28]. This procedure gives a relative accuracy of about 10 %.

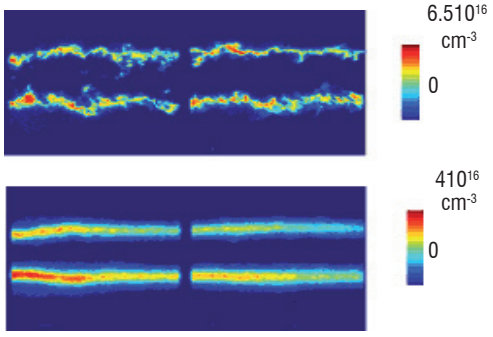

Figure 7 - Instantaneous (a) and averaged (b) PLIF images of OH concentration in a supersonic H_2/air flame at Mach 2. The size of the image is 100x50 mm^2

An example of instantaneous OH distribution recorded in the reactive mixing layer is shown in Figure 7a. The flow goes from left to right; the hydrogen core flow is surrounded by a coaxial air stream. The OH radical, and therefore the reaction zone, is confined in a narrow region along the shear layer on both sides of the hydrogen jet. As the flowfield develops downstream, the reaction zone widens up slightly. Small turbulence length scales of the combustion flow together with large coherent structures are clearly visible on the single-shot images. The structure of the instantaneous flame front consists of thin filaments tightened to the OH-concentrated pockets. The dimensions of these structures are on the order of the diameter of the injection nozzle. In Figure 7b, images averaged over 60 instantaneous frames show a small expansion of the reaction zone with axial distance. It mainly results from the unsteady nature of the flame. The average thickness of the flame is relatively constant and of the order of 6 mm, which is consistent with the size of the structures observed in the instantaneous images. The average reaction zone also presents a wavy shape with a typical spatial period of 50 mm, which can be explained by the presence of compression and expansion waves related to small discontinuities at the combustor walls. The average OH concentration decreases along the flow, confirming weak combustion efficiency related to poor mixing between hydrogen and air. Different fuel injection systems are also tested in order to evaluate their effect on the flame structure and location inside the combustion chamber. For instance, illustrations of the time evolution of the flame structure are displayed with axial fuel injection (movie-axial injection supersonic combustor) and wall fuel injection (movie-wall injection supersonic combustor). Note that the OH-PLIF images are recorded at a frequency rate of 4 Hz. Wall fuel injection exhibits better combustion efficiency due to improved mixing between fuel and air.

Plasma-assisted ignition and combustion

The control of ignition and combustion processes in aircraft jet engines is of significant importance for their performance and reliability. Reduction in ignition delay time, high altitude flame-holding, flame stability improvement and extension of blow-off limits are some of the key factors that are commonly controlled, with limited success, by systems based on conventional thermal ignition mechanisms (arc discharge, etc.). Alternative mechanisms can also trigger a better ignition on modifying the chemical reaction kinetics generated by large electron number densities. Better efficiency of population transfer within electronic and vibrational states can also be obtained using pulsed nanosecond discharges which handle weak reduced electric fields [29-31]. Relevant examples, in this regard, are the experimental studies focused on the influence of nanosecond pulse duration discharges on various phenomena such as reduction in ignition time [32], flame stabilization [33-34], ignition and flame holding [35-36]. However, the mechanisms of energy transfer between the plasma and the gas medium are still not fully understood. Experimental data characterizing the thermodynamic and kinetic processes governing this energy transfer are required for this. More specifically, the population distributions of neutral molecules and species composition are key scalar parameters which need to be used as input parameters for the simulation of these mechanisms. The analysis of the thermodynamic and kinetic mechanisms of fuel oxidation and ignition by a nanosecond pulsed discharge is presented here.

The probing of the pulsed discharge of a high voltage, nanosecond pulse duration, sustained in atmospheric premixed methane-air flows, was performed using laser diagnostics which allows for locally and temporally resolved measurements of temperature and species concentration. Among these diagnostics, coherent anti-Stokes Raman scattering (CARS), laser Thomson scattering (LTS) and planar laser-induced fluorescence (PLIF) were specifically developed and applied to characterize this discharge. CARS [56] was initially used to measure, within the plasma produced in various methane/air mixtures, the population distribution of N_2 in its electronic ground state [37]. Temporal evolution of the rovibrational populations was recorded by delaying the laser shots relative to the discharge pulse (from 10 ns to 1 ms). Experiments were carried out in premixed CH_4/Air flames to study the effect of the nanosecond discharge on ignition and stabilization of combustion at atmospheric pressure. These results were used to assess the feasibility of single-shot CARS measurements of temperature in order to highlight the thermodynamic and kinetic mechanisms of nanosecond discharges in hydrocarbon/air premixed mixtures. Results show that energy transfer induced by collisions of N_2 with the fuel or its decomposition products considerably increases the thermal heating of neutral molecules at temperatures up to 2500 K. The effect of the discharge on the local temperature then leads to the ignition of the CH_4/air mixture for equivalence ratios between 0.7 and 1.3. This work was completed by probing the conversion of the hydrocarbon fuel as well as the kinetic mechanism of recombination of radicals and atoms into neutral molecules such as H_2 and C_2H_2 in situations where no ignition occurs ($\Phi < 0.7$ and $\Phi > 1.3$). Laser Thomson scattering has been implemented to characterize the electric properties of the discharge such as electron density and electron temperature [38]. Results demonstrate that this nanosecond discharge can be classified in the range of weakly ionized plasmas with a reduced electric field of about 250, indicating a small production of ionized molecules. It is also known that nanosecond discharges can trigger a much more effective non-thermal ignition mechanism. This non-thermal ignition mechanism implies that specific plasma-generated active species - radicals, excited atoms and molecules, charged particles, and so on - stimulate the chain reactions of fuel oxidation leading to the ignition of the fuel-oxidizer mixture. In order to evaluate these effects, the temporal distributions of OH and CH within the discharge were measured using PLIF.

The laser system consists of a Nd:YAG laser (YG780, Quantel) combined with a dye laser (TDL 70, Quantel). For OH-PLIF measurements, Rhodamine 590 dye diluted in ethanol solvent is pumped by the Nd:YAG laser. The laser is tuned to the Q1(5) transition of the (1,0) band of the $A^2\Pi^+ - X^2\Sigma$ system of OH at 282.75 nm. Fluorescence from the A-X(1,0) and (0,0) bands is collected with an UV-Nikkor 105 mm/F=4.5 lens and imaged onto an intensified CCD camera (PIMAX, 1024x1024 pixels). Dichroic and WG295 optical glass filters are used to detect the fluorescence of the OH radical in the 306–312 nm spectral range and to reject plasma emission and incident light. For CH-PLIF measurements, the P1(10) transition of the $C^2\Sigma^+ - A^2\Pi(0,0)$ located at 317.30 nm is excited. This excitation wavelength is obtained using Rhodamine 610 diluted in ethanol solvent. Collection of fluorescence from the C-X(0,0) band located between 313 and 318 nm is obtained by using a dichroic filter centered at 313 nm and presenting a HWHM of 5 nm. For both measurements, the laser beam is shaped into a 150 μm vertical sheet with 3 mm height, corresponding to the distance between the two electrodes. Therefore, spatial resolution is limited to 20 μm x 20 μm x 150 μm. Optimization of the filtering of the fluorescence signals is performed with an image intensifier gate of 20 ns. As for the CARS measurements, the measurements are performed for various equivalence ratios surrounding the limits of ignition in order to well isolate the chemical mechanisms produced by the discharge from those induced by combustion.

Plasma-generated OH radicals were confirmed throughout the discharge volume between the electrodes. Figure 8 shows a typical instantaneous OH distribution recorded over a cross section in the middle of the streamer 20 μs after the high-voltage pulse. It is noted that OH production is quite homogeneous within the discharge. Observation of the OH spatial structures shows local disturbances close to the electrodes which probably arise from additional electrically-enhanced surface catalytic reactions and/or local joule heating of the electrode enhancing the heat release. This last effect is highlighted in the (movie-OHPLIF) presenting the time evolution of OH for delay times ranging from 0 to 300 μs.

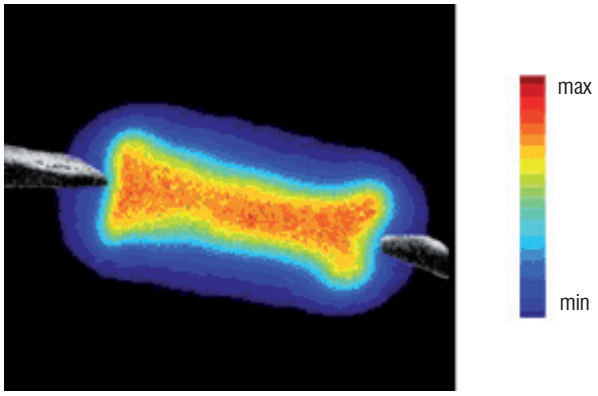

Figure 8 - Example of OH laser-induced fluorescence spatial distribution recorded between the electrodes 20 μs after the discharge

From the fluorescence images recorded at various times, the temporal evolution of OH fluorescence has been deduced for four equivalence ratios and the results are presented in Figure 9. First of all, OH production is observable at a time less than 10 ns in a very lean gas mixture (Φ=0.05). This species subsists at similar concentrations up to a time of 1 μs. After this time period, significant production of OH is observed with a peak located at 20-30 μs. Then, the OH fluorescence decreases and totally disappears after ~200-300 μs. In the lean-regime condition (i.e. equivalence ratio ranging from 0.5 to 0.65), a considerable increase of OH fluorescence is now observed when adding CH_4 into the gas mixture. The OH fluorescence continuously increases between 500 ns and 1μs, then OH distributions exhibit a flat profile over a period not exceeding 30 μs. The simultaneous presence of peaks of OH and temperature at a delay of 500 ns also represents favorable conditions of ignition of the gas mixture when increasing the equivalence ratio to 0.7 [37]. The relaxation of the OH population to the ground state is also noted. The maximum amount of OH is multiplied by a factor of 10-12, demonstrating the effectiveness of the plasma to produce large amounts of OH radicals compared with the case of Φ=0.05. For a rich CH_4/air mixture, fast production of OH is still observed up to a period of 20 ns. Then, OH fluorescence exhibits a flat profile over a period of 800 ns and finally decreases continuously to a time of ~20-30 μs. Comparison of these temporal distributions with temperature measurements recorded in the same conditions [37] also shows a strong correlation. In a very lean regime, the common increase of OH and rotational temperature arising from exothermic recombination reactions with transient species like O or H atoms, is observed. In the lean

regime ($0.5<\Phi<0.65$), similar correlations between temperature and production of OH radicals are also noted, indicating the existence of exothermic chemical fuel oxidation mechanisms triggered by plasma-generated radicals and leading to flow heating at temperatures up to 2500 K. Finally, the fast decrease of OH in the rich mixture is piloted by the efficient relaxation of energy into the plasma.

Figure 9 - Temporal Evolution of OH laser-induced fluorescence for various equivalence ratios

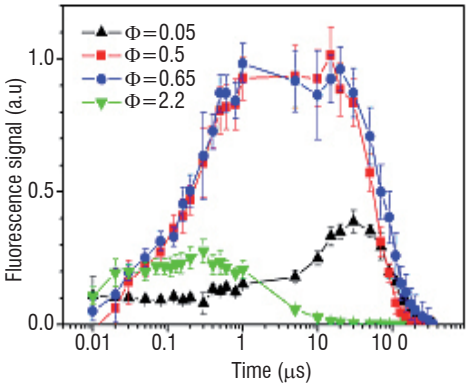

Preliminary experiments for CH detection using PLIF were also carried out in the same conditions as for OH. CH production is also observed within the discharge, indicating an efficient decomposition of the fuel by the plasma. For example, Figure 10 shows a typical instantaneous CH distribution recorded in a cross section in the middle of the discharge. This measurement was recorded 500 ns after the high-voltage pulse. Contrary to OH, the spatial distribution of CH fluorescence between the electrodes is not homogeneous. CH is observed along two thin regions located at the periphery of the plasma sheath. Analyzing the CH fluorescence images with the same method as for OH allows for measurement of the temporal behavior of the CH fluorescence.

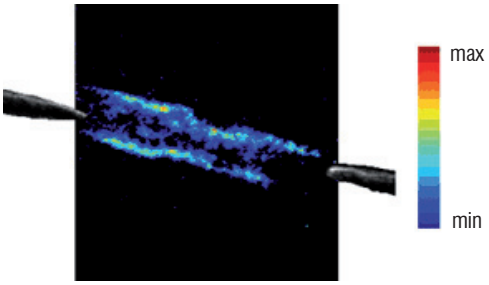

Figure 10 - Instantaneous CH laser-induced fluorescence distribution recorded between the electrodes 500 ns after the discharge

Figure 11 shows the temporal evolution for a rich CH_4/air mixture. After a large production of CH at a time less than 10 ns, the CH fluorescence signal decreases progressively until 100 ns. A flat profile with a small rising of CH at ~500-600 ns is then observed. CH radicals then continue to decrease before totally disappearing after ~10-20 μs. The temporal behavior of CH production, with a reduction of its total intensity, is found to be similar when using equivalence ratio close to the upper limit of ignition ($\Phi=1.3$). The amount of CH radical measured at very short durations yields a drastic enhancement of the initiation chemical mechanisms and subsequently the chain chemical reactions inside the gaseous flowfield. This effect, combined with the fast increase of temperature, exhibits a significant reduction in ignition time (~500 ns) and increases lean burn capability relative to conventional spark ignition [38]. For instance, the sequence of ignition and development of the flame downstream from the electrodes is displayed on the (movie-ignition OH) which presents the temporal evolution of the flame structure (represented by the OH* radical chemiluminescence) over a discharge cycle ($\Delta T=10$ ms) recorded in an atmospheric CH_4/air mixture with an equivalence ratio of 0.95. These results also confirm the numerical analysis of plasma simulation by Campbell and Egolfopoulos (2005) who investigated the kinetic paths to radical-induced ignition of CH_4/air mixtures [39]. In particular, the analysis of the kinetic mechanism evolution to the ignition by adding CH_3, CH_2, CH, and C (up to a few percent) demonstrates the key role of CH radicals, which rapidly oxidized to HCO, as the most effective in stimulating ignition through a chain mechanism.

Figure 11 - Temporal Evolution of CH laser-induced fluorescence for an equivalence ratio of 2.2

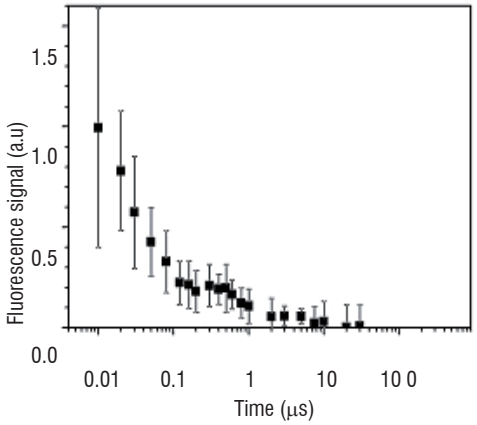

Multiphase chemistry and dynamics applications

Measurement in multiphase flows

By contrast with PLIF using ketone added to pure fuels for temperature and species concentration measurements in basic experiments, the probing of natural fluorescent tracers already present in commercial fuels will now be discussed. This concerns for example aeronautic fuel (kerosene or Jet A1) in which aromatics are naturally present in the species composition. From the pioneering work of Baranger et al. [23], it has been demonstrated that a kerosene vapor fluorescence spectrum excited with a 266 nm wavelength is composed of two fluorescence bands which vary differently with temperature, pressure and oxygen quenching. Identification of the fluorescent species has been performed and the two bands have been respectively attributed to the single-ring aromatics (1,2,4-trimethylbenzene) and the two-ring aromatics like naphthalene and its derivatives. Detection of fluorescence from aromatics with a single excitation wavelength over two specific spectral ranges can then provide dual-parameter imaging, yielding for example equivalence ratio in addition to temperature. Collection of mono-aromatic and di-aromatic fluorescence signals on two separate ICCD cameras with appropriate spectral filters may be one of the possibilities thanks to their different temperature and oxygen dependencies. Using experimentally-determined behavior of both fluorescence bands, along with a calibration point in a reference flow where thermodynamic parameters are well known, an iterative processing routine of both instantaneous fluorescence signals, combined with the closure relation for species composition is then used to determine the desired quantities. Note that this data reduction implies that the

ratio between mono-aromatics and di-aromatics remains constant during the experiments. This assumption remains valid for temperatures up to 1100-1300 K, where kerosene pyrolysis is observed.

Figure 12 - (a) Fluorescence raw image of the liquid and vapor phases of kerosene, (b) equivalence ratio at the outlet of a LPP injector (air inlet temperature: 580 K, overall equivalence ratio: 0.44, atmospheric pressure). The size of the image is 35x50 mm^2

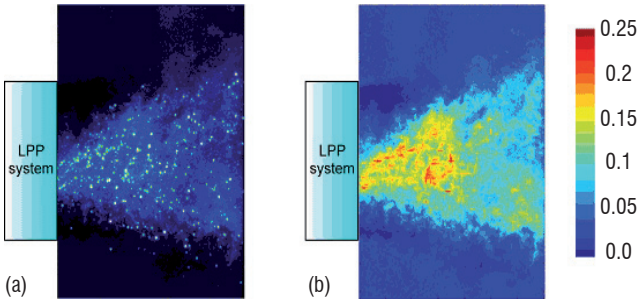

Figure 12a represents a typical single-shot image of fluorescence from kerosene droplets and vapor by kerosene-PLIF, recorded at the outlet of a lean premixed pre-vaporized (LPP) injector. This new type of injector is used in helicopter engines in order to improve the atomization and evaporation of liquid kerosene and to increase mixing between kerosene vapor and the surrounding air prior to combustion [40]. The idea underlying this concept is to burn a fuel/air mixture as lean as possible in order to reduce pollutant emissions. The goal of the experiment is to quantify the ability of the injector to provide a homogeneous fuel/air mixture with a low equivalence ratio. The experiments are carried out for evaporating conditions, without combustion. The picture size is 35x50 mm^2, the kerosene/air flow comes from the left hand side. Kerosene fuel is directly probed via the detection of aromatics, and therefore the current experiment does not require any added tracers. The bright dots, representing large intensities, correspond to droplets, while fuel vapor is displayed with a false blue-to-green color scale. Due to the difference of density between the liquid and vapor phases of kerosene, fluorescence signals are significantly larger for the liquid phase. As a result, there is a strong intensity gradient between a droplet and its surrounding vapor. Therefore, it is possible to take advantage of this feature to discriminate the liquid and gas phases and to identify the location of the droplets. Data processing using a calibration point in a reference flow allows us to obtain instantaneous two-dimensional maps of the equivalence ratio at the outlet of the injector, Figure 12b. As can be seen, the kerosene/air jet is fairly directional and exhibits some radial expansion with axial distance. In addition, kerosene vapor remains mainly located along the combustor centerline, which may be due to swirl effects which create a “shield” that prevents kerosene vapor from reaching a large radial location.

Combustion of isolated droplets

Spray vaporization and combustion are very complex topics which require an understanding of physical processes such as spray atomization and transport, turbulence and chemistry. Nonetheless, in an industrial-type burner, all these parameters interact with each other, which prevents determination of their separate influences. As a result, experiments are often carried out on idealized sprays in order to minimize the coupling between the different effects and to provide parametric results. The simplest geometry consists of studying the evaporation or combustion of suspended hydrocarbon droplets [41-44]. Another possibility is to consider porous spheres [45-46], which are particularly used for temperature measurements and determination of chemical species during droplet combustion. However, both of the aforementioned types of experiments make use of large droplets, of the order of few millimeters, which are not representative of real sprays. Streams or arrays of mono-dispersed droplets have also been frequently used in basic studies on sprays, for example to determine the influence of the spacing parameter on droplet combustion [47-49]. This simple geometry is particularly attractive because it generates a temporally and spatially repeatable stream of droplets with well-controlled injection frequency, droplet size and velocity and droplet spacing, which allows us to study the individual influence of each of these parameters on droplet vaporization. Physical models can be derived from such experiments and can be subsequently implemented in simulation codes in order to run more complex situations.

Figure 13 - Spatial distribution of OH radical laser-induced fluorescence around a burning droplet for different droplet combustion regimes: stationary envelope flame (a), envelope flame around a moving droplet (b-d), wake flame (e) and boundary-layer flame (f). Size of the image is 2x2 mm^2 [50]

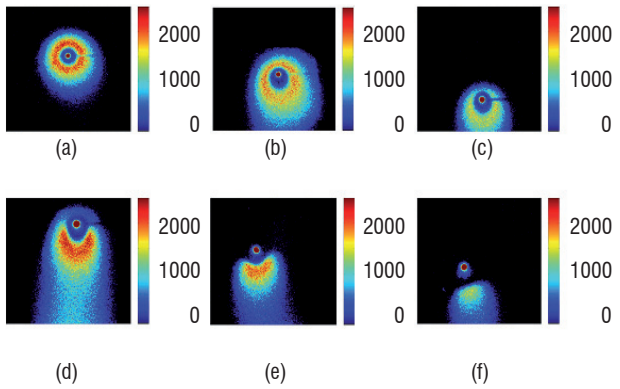

OH-PLIF imaging with high spatial resolution is used in a laminar diffusion counterflow burner fuelled with methane to provide information on isolated droplet combustion [50]. Measurements are performed on the oxidizer side at 10 mm above the flame front on the burner axis. The resulting images are presented with a false colorscale to display areas of fuel vapor phase and OH radical around droplets on the most suitable range. As a consequence, fluorescence signals from liquid acetone droplets, which are typically two orders of magnitude higher than the vapor one, appear to be uniform and at the maximum value of the colorscale. Figure 13 shows the OH distributions recorded with the magnification ratio of 1:1.2 and illustrates the effect of the droplet Reynolds number on isolated droplet combustion. Different burning regimes, from the configuration of the envelope flame to that of the boundary-layer flame, are obtained for droplet Reynolds numbers between 10 and 40. Typical envelope flames around the droplet are illustrated in Figures 13a-13c. In particular, the perfectly spherical shape of the flame around the droplet in Figure 13a indicates the combustion regime of a stagnant droplet. This regime is observed when the droplet, after its ignition through the flame front, reaches the top of its ballistic trajectory (i.e. when the droplet has an axial velocity equal to ≈0). By contrast, in Figures 13b and 13c, a stretching of the flame behind the droplet is observed, which suggests that fuel vapor is not distributed in a spherical manner around the droplet, hence that these droplets are moving. Comparison between Figures. 13b and 13c also shows that the OH concentration peak is first located ahead of the

droplet and then gradually switches to the region behind the droplet. This transition characterizes the evolution of the flame reaction rate around a burning droplet injected in an airflow with bulk direction opposed to droplet motion. A noticeable reduction of the flame front thickness ahead of the droplet is also observed, which suggests that fast cooling occurs on the top of the flame due to the counterflowing air stream. In Figure 13d, the flame is extinguished ahead of the droplet and in Figure 13e, the transition has occurred and the envelope flame is now replaced by a wake flame. Due to flame front extinction ahead of the droplet, the counterflowing air stream penetrates the recirculation zone behind the droplet and mixes with fuel vapor present in that region. An increase in OH intensity behind the droplet is also observed in Figures 13d and 13e, which suggests that the droplet burning rate may be enhanced by the change of combustion regime from envelope to wake flame. In Figures 13f, a boundary-layer flame replaces the wake flame and combustion only takes place in the droplet puff. In this situation, flame stability is strongly reduced and extinction occurs very easily. Compared with the previous wake flame, OH fluorescence intensity and flame thickness strongly decrease while the distance between droplet surface and the flame front increases by roughly 60 %. It is noteworthy that the current study presents good agreement with the numerical results from Jiang et al. [51] and Liu et al. [52] which were obtained with 100 and 200 μm n-octane droplets respectively. In particular, the occurrence of various droplet combustion regimes is clearly identified in the present experiments for droplet Reynolds number of the same order as that from Liu et al. [52]. Experimental evidence of the different combustion regimes has been reported in the literature for large droplets [46-47] or porous spheres [53] with diameters of several millimeters. However, to the best of our knowledge, this is the first time that the phenomena have been observed with OH-PLIF for droplets that are representative of real sprays.

The influence of droplet dynamics on the counterflow flame front also shows that the flame front can be strongly distorted by the droplet crossing. For instance, the different steps of the local extinction mechanism of the CH4/air flame by a droplet are presented in the (movie-droplet without flame). Note that the images of this sequence are not recorded in real-time because of the limited acquisition rate of the ICCD camera (3 Hz) compared to the duration of the event (few ms). This sequence is reconstructed by selecting OH images recorded from different series of measurements. The velocity of a droplet entering the flame front is estimated from Figure 13f which corresponds to the case where a boundary-layer flame is present behind the droplet. This physical process, considered as the limit case before the droplet extinguishes, occurs for a droplet velocity of about 2 m/s. Consequently, droplets crossing the flame front have velocities higher than this value. As seen in the movie, droplets with high velocity lead to local extinction of the flame front. By contrast, droplets with lower velocity can ignite within the flame front and burn on the oxidizer side (movie-droplet with flame).

Kerosene spray combustion in practical combustion systems

This application highlights the potential of PLIF to simultaneously measure several scalar quantities in practical combustors at high pressure. The goal of the present experiments is to combine kerosene-PLIF and OH-PLIF described previously in order to simultaneously measure the local equivalence ratio and flame front structure in a fired high-pressure combustor operating with Jet A1 fuel. The spatial and temporal correlation between fuel vapor distribution and flame structure are measured to evaluate the influence of fuel concentration on the local flame reaction rate. The techniques are successfully applied at pressures of up to 2.2 MPa [54].

The combustor used in the experiments is the so-called “M1 test bench”, which is the high temperature-high pressure combustion facility at Onera dedicated to the investigation of aircraft and helicopter injectors under real operating conditions. This bench can preheat air up to 900 K for flowrates up to 4 kg/s. Preheated air is injected into the combustor together with liquid kerosene via a new multipoint injector designed by the French company SAFRAN: a single pilot injector is located on the combustor axis and it is used to stabilise the flame whereas a multipoint main injector is located at a larger radial distance. The fuel flowrate is split between both injectors and the ratio between equivalence ratios from the pilot and the main injector (Φ_{pilot}/Φ_{main}) lies between 0.1 and 1, except for a condition where only the pilot injector is used. The combustor comprises a water-cooled visualization sector which is equipped with optical accesses for laser measurements. The outlet of the combustor is equipped with a sonic throttle which can be partly obstructed by a water-cooled needle in order to control the pressure inside the combustor. The air inlet temperature varies between 480 and 730 K and the pressure inside the combustor is in the range of 0.45–2.2 MPa.

Two laser systems are used to perform OH and kerosene vapor PLIF measurements simultaneously. Measurements for the OH radical are performed by exciting the Q1(5) line of the (1, 0) band of the OH ($X^2\Pi$ - $A^2\Sigma^+$) system. Measurements of kerosene fluorescence use a single-excitation scheme which comprises a frequency-quadrupled Nd:YAG laser generating 8 ns, 50 mJ pulses at 266 nm. The time delay between the two laser beams is set at 200 ns in order to avoid cross-talk between fluorescence signals from the OH radical and the kerosene. This duration is found to be much shorter than the typical flow timescales, ensuring that images of OH and kerosene fluorescence are representative of the same phenomenon at the time of recording. Both laser beams are transported via optical mirrors around the combustor facility and superimposed with a combination of dichroic mirrors. They are then transformed into two superimposed collimated sheets using a unique set of cylindrical and spherical lenses. The fluorescence from the OH radicals is recorded with a 16-bit ICCD camera while the fluorescence from the kerosene vapor and liquid phases is simultaneously recorded by two 16-bit ICCD cameras. The camera used for OH visualization has a CCD array of 1024x1024 pixels, a temporal gate of 40 ns, with a framing rate of 4 Hz and it is equipped with a 105 mm, f/4.5 UV-NIKKOR lens. The cameras used for kerosene detection have a CCD array of 512x512 pixels, a temporal gate of 40 ns, with a framing rate of 4 Hz, and each camera is equipped with an achromatic UV lens. For OH measurements, the camera has a combination of glass filters (WG 295 and UG 5) and an interferential filter centered at 310 nm. For kerosene measurements, the first camera is equipped with a combination of glass filters to collect the whole fluorescence from mono- and di-aromatics, whereas the second camera uses a combination of glass filters to collect fluorescence from di-aromatics only.

Figure 14 shows typical radial single-shot images of kerosene and OH fluorescence for the condition where the pilot and the main injectors are operated at 0.95 MPa with the same equivalence ratio. The laser sheet propagates across the combustor, perpendicular to the injection system. Images are corrected for distortion due to the angle of observation ($\sim 30°$) between the laser sheet and the ICCD cameras. It is noticed that the flame front exhibits a double structure:

one is close to the combustor axis and comes from the pilot injector, whereas the peripheral flame front can be attributed to the main injector. Comparison of Figures 14a and 14b shows that kerosene is located at a larger axial distance than the OH radical, which indicates that combustion occurs on the inner side of the cone delimiting the kerosene. Finally, the spatial distribution of both kerosene and the OH radical are axisymmetric, which confirms another result of the axial measurements. This suggests that such a multi-point injector can provide a fairly homogeneous distribution of kerosene in the combustor. Regions with large gradients of fuel concentration should therefore be limited, which may help to achieve stable combustion and low levels of pollutant emissions.

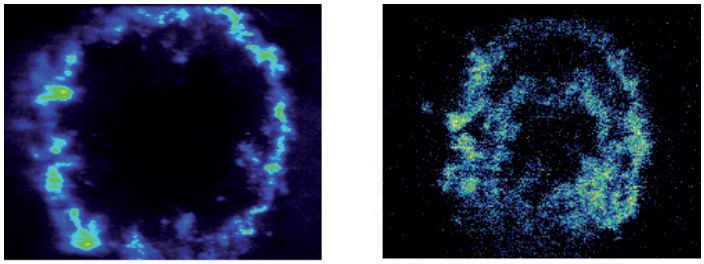

(a) (b)

Figure 14 - Radial instantaneous fluorescence images of (a) kerosene and (b) OH radical at the outlet of a multipoint injector (Air inlet temperature: 590 K, pressure: 0.95 MPa, $\Phi_{pilot}/\Phi_{main}=1$). The size of the image is 50x50 mm^2 [54]

Conclusion, future outlook

PLIF imaging diagnostic is a powerful tool for the understanding of fluid dynamics and combustion physics which can enhance the research and development process. There has been a remarkable increase in PLIF diagnostic capability over the last two decades, and the field continues to develop at a fast pace. Its capabilities go far beyond the mere observation of two-dimensional signal intensities. The development status of PLIF has now passed the threshold between qualitative and quantitative images. Nowadays, both in laboratory research and practical combustion, PLIF is well-suited to a wide variety of applications performed at high pressures and temperatures relevant to real engines and gas turbines.

In the near future, the availability of new laser sources operating at high frequency rates, detectors, and data processing schemes will allow for the acquisition of more accurate data, and measurements that could be more specifically tailored to the needs of the modeling community. One orientation, which is already underway in different research laboratories, will involve the development of 2D and 3D time-resolved planar imaging and simultaneous measurements of multiple scalars. The data collected will help to uncover yet undetected physical processes in turbulent combustion for which new models can be elaborated. For example, time-sequenced imaging of combustion instabilities in Internal Combustion (IC) engines, ultra-lean gas turbines, new aircraft injection systems and re-ignition at high altitude with laser and plasma igniters will provide significant insight into the immensely complex flows prevailing in these combustors. In a similar way, multi-scalar diagnostics will provide significant contributions to our understanding of turbulent combustion and, in particular, the effects of turbulent mixing on flame chemistry. Multi-scalar data, combined with velocity measurements, will constitute a quantitative database for testing advanced models of multiphase turbulent combustion. The scalars of interest include temperature, fuel molecules, key intermediate combustion species, pollutant precursors (PAH) and pollutants like aldehydes, NOx and CO. Successful implementation of PLIF is expected to provide high quality experimental data for traditional and emerging fuels (biofuels), which can be used as a benchmark for developing and validating the predictive capability of combustion models in engines and gas turbines ■

Acknowledgements

The authors are greatly indebted to their former co-workers A. Bresson, P. Baranger, B. Rossow, D. Messina and G.A. Grandin as well as the Direction Générale de l'Armement (DGA) and the French industrialist SAFRAN for financial support of many projects providing important input to combustion analysis by PLIF.

References

[1] R.K. HANSON - *Combustion Diagnostics: Planar Imaging Techniques.* Proc. Combust. Inst., (1986) 1677-1691.
[2] R MILES - *Flow-field Diagnostics, Applied Combustion Diagnostics.* Edited by Katharina Kohse-Höinghaus & Jay Jeffries, Taylor and Francis Publishers (2002).
[3] A.C ECKBRETH - *Laser Diagnostics for Combustion Temperature and Species.* 2nd edition, Gordon and Breach Publishers, Amsterdam (1996).
[4] A.H. EPSTEIN - *Quantitative Density Visualization in a Transonic Compressor Rotor.* J. Energ. Power 99 (1977) 460-475.
[5] G. KYCHAKOFF, R.D. HOWE, R.K. HANSON - *Quantitative Flow Visualization Technique for Measurements in Combustion Gases.* Appl. Opt. 23 (1982) 704-712.
[6] R.K. HANSON, J.M. SEITZMAN, P.H. PAUL - *Planar Laser Fluorescence Imaging of Combustion Gases.* Appl. Phys. B50 (1990) 441-454.
[7] K. KOHSE-HOÏNGHAUS - *Laser Techniques for the Quantitative Detection of Reactive Intermediates in Combustion Systems.* Prog. Energ. Combust. 20 (1994) 1-203.
[8] J.W. DAILY - *Laser Induced Fluorescence Spectroscopy in Flames.* Prog. Energy Combust. Sci. 23 (1997) 133-199.
[9] J.E. BROADWELL, P.E. DIMOTAKIS - *Implications of Recent Experimental Results for Modelling Reactions in Turbulent Flows.* AIAA Journal, 24 (1986) 885-889.
[10] A. YARIV - *Quantum Electronics.* Wiley, New York (1975).
[11] W. DEMTRÖDER - *Laser Spectroscopy.* Springer, Berlin Heidelberg, (1982).
[12] E.H. PIEPMEIER - Spectros. Chimi. Acta 27b (1972) 431-443.

[13] N.M. LAURENDEAU - Prog. Energy Combust. Sci. 14 (1988) 147-170.
[14] B.K. MCMILLIN, J.L. PALMER, R.K. HANSON - *Temporally Resolved, Two-line Fluorescence Imaging of NO Temperature in a Transverse Jet in a Supersonic Crossflow.* Appl. Opt. 32 (1993) 7532-7545.
[15] K.A. WATSON, K.M. LYONS, J.M. DONBAR, C.D. CARTER - *Scalar and Velocity Field Measurements in a Lifted CH4-air Diffusion Flame.* Comb Flame, 117 (1999) 257-271.
[16] H.B. NAJM, P.H. PAUL, C.J. MUELLER, P.S. WYCKOFF - *On the Adequacy of Certain Experimental Observables as Measurements of Flame Burning Rate.* Comb. Flame, 113 (1998) 312-332.
[17] P.H. PAUL, H.B. NAJM - *Planar Laser Induced Fluorescence Imaging of Flame Heat Release Rate.* Proc. Comb. Inst. (1998) 43-50.
[18] C. SCHULZ, V. SICK, *Tracer LIF Diagnostics: Quantitative Measurements of Fuel Concentration, Temperature and Fuel/air Ratio in Practical Combustion Systems.* Prog. Energy Combust. Sci. 31 (2005) 75-121.
[19] H. NEIJ - *Development and Demonstration of 2D-LIF for Studies in SI Engines.* Comb. Flame 99 (1994) 449-457.
[20] D. WOLFF, H. SCHLÜTER, V. BEUSHAUSEN, P. ANDRESEN - *Quantitative Determination of Fuel Air Mixture Distributions in an Internal Combustion Engine using PLIF of Acetone Ber. Buns.* Phys. Chem. 97 (1993) 1738-1741.
[21] F. GRISCH, M.C. THURBER, R.K. HANSON - *Mesure de température par fluorescence induite par laser sur la molécule d'acétone.* Revue Scientifique et Technique de la Défense, 4 (1997) 51-60.
[22] M.C. THURBER, F. GRISCH, R.K. HANSON - *Temperature Imaging with Single and Dual-Wavelength Acetone Planar Laser-Induced Fluorescence.* Opt. Lett. 22 (1997) 251-253.
[23] P. BARANGER, M. ORAIN, F. GRISCH - *Fluorescence Spectroscopy of Kerosene Vapor: Application to Gas Turbines.* AIAA Paper 2005-828, 43rd AIAA Aerospace Sciences Meeting and Exhibit, Reno, Nevada, (2005).
[24] J. GUIDEZ, C. DUMAND, T. COURVOISIER, M. ORAIN - *Specific Problems of Micro Gas Turbine for Micro Drones Application.* ISABE Paper 2005-1273, ISABE Conference, Munich (2005).
[25] M.C. THURBER, F. GRISCH, B. J. KIRBY, M. VOTSMEIER, R.K. HANSON - *Measurements and Modeling of Acetone Laser Induced Fluorescence with Implications for Temperature-imaging Diagnostics".* Appl. Optics, 37 (1998) 4693-4978.
[26] A. BRESSON, P. BOUCHARDY, P. MAGRE, F. GRISCH - *OH/acetone PLIF and CARS Thermometry in a Supersonic Reactive Layer.* AIAA paper 2001-1759, 10th AIAA/NAL/NASDA/ISAS International Space planes and hypersonic Systems and technologies conference, Kyoto, Japan, 2001.
[27] R.J. KEE, F.M. RUPLEY, J.A. MILLER - Sandia National Lab. Rep. SAND89-8009, 1989.
[28] R.J. KEE, J.F. GREAR, M.D. SMOOKE, J.A. MILLER - Sandia National Lab. Rep. SAND85-8240, 1985.
[29] A. BOGAERTS, E. NEYTS, R. GIJBELS, J. VAN DER MEULEN - *Gas Discharge Plasmas and their Applications.* Spectrochemica Acta Part B 57 (2002) 609-658.
[30] C. H. KRUGER, C. LAUX, L. YU, D. PACKAN, L. PIERROT - *Nonequilibrium Discharges in Air and Nitrogen Plasmas at Atmospheric Pressure.* Pure Appl. Chem. 74 (2002) 337-347.
[31] S.M. STARIKOVSKAYA, J. PHYS - D: Appl. Phys. 39 (2006) 265-299.
[32] A.M. STARIK, N.S. TITOVA, L.V. BEZGIN, V.I. KOPCHENOV - *Initiation of Diffusion Combustion in a Supersonic Flow of H2-air Mixture by Electrical-Discharge-Excited Oxygen Molecules.* J. Phys. D: Appl. Phys. 41 (2008) 125210 (12pp).
[33] E.I. MINTOUSSOV, S.V. PANCHESHNYI, A.YU. STARIKOVSKII - AIAA Paper 2004-1013, 42nd AIAA Aerospace Sciences Meeting and Exhibit, Reno, NV, January 2004.
[34] W. KIM, H. DO, M.G. MUNGAL, M.A. CAPPELLI - Proc. Combust. Inst..(2007) 3319-3326.
[35] S. PANCHESHNYI, D.A. LACOSTE, A. BOURDON, C. LAUX - AIAA Paper 2006-3769, 37th AIAA Plasmadynamics and Lasers Conference, San Francisco, CA, June 2006.
[36] G. LOU, A. BAO, M. NISHIHARA - Proc. Combust. Inst. (2007) 3327-3334.
[37] D. MESSINA, B. ATTAL-TRÉTOUT, F. GRISCH - *Analysis of a Non-Equilibrium Pulsed Nanosecond Discharge at Atmospheric Pressure using Coherent anti-Stokes Raman Scattering.* Proc. Combust. Inst. (2007) 825-832.
[38] D. MESSINA, G.A. GRANDIN, B. ATTAL-TRÉTOUT, F. GRISCH - *Laser-Based Measurements of Gas-Phase Chemistry in Non-Equilibrium Pulsed Nanosecond Discharges.* 2nd Colloque INCA, CORIA, Rouen (France), 2008.
[39] C.S. CAMPBELL, F.N. EGOLFOPOULOS - *Kinetics Paths to Radical-induced Ignition of Methane/air Mixtures.* Combustion Science and Technology, 177 (2005) 2275-2298.
[40] M. ORAIN, F. GRISCH - *Equivalence Ratio Measurements in Kerosene-Fuelled Combustors Using Planar Laser-Induced Fluorescence: Comparison between LP and LPP Injectors.* Paper 136, 2nd European Conference for Aero-Space Science (EUCASS), Brussels (Belgium), July 2007.
[41] G.A.E. GODSAVE - *Burning of Fuel Droplets.* 4th Int. Symp. on Comb. (1952) 818-830.
[42] S. OKAJIMA, S. KUMAGAI - *Further Investigations of Combustion of Free Droplets in a Freely Chamber Including Moving Droplets.* Proc. Combust. Inst. (1976) 401-407.
[43] J.J. WHANG, C.Y. YUKAO, J.T. HO, S.C. WONG - *Experimental Study of the Ignition of Single Droplets under Forced Convection.* Comb. and Flame, 110 (1997) 366-376.
[44] T. SUEKANE, K. YASUTOMI, S. HIRAI - *Experimental Observation of Effects of Convection on Flame Shape and Extinction on N-Heptane Single Droplets.* Comb. and Flame, 126 (2001) 1599-1601.
[45] D.B. SPALDING - *The Combustion of Liquid Fuels.* Proc. Combust. Inst. (1952) 847-864.
[46] S. R. GOLLAHALLI, T.A. BRZUSTOWSKI - *Experimental Studies on the Flame Structure in the Wake of a Burning Droplet.* Proc. Combust. Inst. (1974) 1333-1344.
[47] J.P. GORE, W.H. MENG, J.H. JANG - *Droplet Flames in Reactive Environments.* Comb. and Flame, 82 (1990) 126-141.
[48] J.J. SANGIOVANNI, M. LABOWSKY - *Burning Times of Linear Fuel Droplets Arrays: A Comparison of Experiment and Theory.* Comb. and Flame, 47, (1982) 15-30.
[49] M. ORAIN, X. MERCIER, F. GRISCH - *PLIF Imaging of Fuel Vapor Distribution around a Monodispersed Stream of Acetone Droplets, Comparison with Modelling.* Combustion Science and Technology, 177 (2005)1-30.
[50] X. MERCIER, M. ORAIN, F. GRISCH - *Investigation of Droplet Combustion in Strained Counterflow Diffusion Flames using Planar Laser-Induced Fluorescence.*

Applied Physics B, 88, (2007) 151-160.
[51] T.L. JIANG, W.H. CHEN, M.J. TSAI, H.H. CHIU - *A Numerical Investigation of Multiple Flame Configurations in Convective Droplet Gasification Flame, Comb. and Flame, 103 (1995) 221-238.*
[52] C.C. LIU, W.H. CHEN, T.L. JIANG - *Model of Unsteady N-Octane Droplet Burning in High-Temperature Streams, Combust.* Sci. and Tech. 176 (2004) 183-213.
[53] V. RAGHAVAN, V. BABU, T. SUNDARARAJAN, R. NATARAJAN - *Flame Shapes and Burning Rates of Spherical Fuel Particles in a Mixed Convective Environment.* Int. J. Heat Mass Transf. 48 (2005) 5354-5370.
[54] F. GRISCH, M. ORAIN, B. ROSSOW, E. JOURDANNEAU, C. GUIN - *Simultaneous Equivalence Ratio and Flame Structure Measurements in Multipoint Injector Using PLIF.* AIAA Paper 2008-4868, 44th AIAA/ASME/SAE/ASEE Joint Propulsion Conference & Exhibit, Hartford, CT (USA), July 2008.
[55] F. DUPOIRIEUX - *Optical Diagnotics Used at Onera to Characterize Turbulent Reactive Flows and to Validate Aero and Rocket Engine Combustor Modeling*. AerospaceLab N°1, October 2009.
[56] B. ATTAL-TRETOUT - *Laser Spectroscopy for in situ Diagnostics.* AerospaceLab N°1, October 2009.

Acronyms
PLIF (Planar Laser-Induced Fluorescence)
LIF (Laser-Induced Fluorescence)
CCD (Charged-Coupled Device)
ICCD (Intensified Charged-Coupled Device)
RANS (Reynold Average Navier Stokes)
LES (Large Eddy Simulation)
CARS (Coherent Anti-Stokes Raman Scattering)
LTS (Laser Thomson Scattering)
LPP (Lean Premixed Pre-vaporized)

Videos : http://www.aerospacelab-journal.org/al1/Role-of-Planar-Laser-Induced-Fluorescence-in-combustion-research

AUTHORS

Frédéric GRISCH, Masters degree in fluid mechanics in 1982, PhD in Energetics in 1988 and HDR in 2008 from the University of Rouen (France). Senior scientist at Onera in charge of the development and application of laser diagnostics (CARS, PLIF, Raman scattering, Rayleigh scattering, Thomson scattering, etc.) for gaseous, liquid and solid propellant combustion, plasmas and nonreactive flow fields. Head of an Onera/CNRS research project on optical techniques for the investigation of multicomponent spray evaporation.

Mikael ORAIN, Masters degree in fluid mechanics in 1996, PhD in Mechanical Engineering in 2001 at Imperial College London (UK). Research scientist at Onera in charge of developing PLIF for the measurement of temperature and species concentration in reacting and non-reacting two-phase flows.